Published as: *Nat Methods*. 2012 December ; 9(12): 1202–1205.

Two-photon optogenetics of dendritic spines and neural circuits in 3D

Adam M. Packer[1,*], **Darcy S. Peterka**[1,*], **Jan J. Hirtz**[1], **Rohit Prakash**[2], **Karl Deisseroth**[2], and **Rafael Yuste**[1]

[1]HHMI, Dept. Bio. Sci., Columbia University, New York, NY 10027

[2]HHMI, Dept. Bioeng., Stanford University, Stanford, CA 94305

Abstract

We demonstrate a two-photon optogenetic method that generates action potentials in neurons with single-cell precision, using the red-shifted opsin C1V1$_T$. We apply the method to optically map synaptic circuits in mouse neocortical brain slices and to activate small dendritic regions and individual spines. Using a spatial light modulator we split the laser beam onto several neurons and perform simultaneous optogenetic activation of selected neurons in three dimensions.

Temporally precise control of neuronal firing with single-cell precision is a long-sought goal in neuroscience. While optogenetics allows optical manipulation of genetically defined populations of neurons[1, 2], typical experiments use visible light, which targets all opsin-expressing neurons simultaneously and does not permit spatio-temporal manipulation of neuronal activity at single cell-level. Two-photon photostimulation offers single-cell resolution[3–6], although it has only been exploited for optogenetics in a few instances[4–7]. Among the reasons for this are the limitations imposed by current opsins. Although Channelrhodopsin-2 (ChR2) has a high two-photon excitation cross-section[4], its single channel conductance is low and it displays fast kinetics [8], so the net charge injected per channel is small. This, combined with the small two-photon excitation volume, means that for two-photon activation of a neuron with ChR2 one needs either very high opsin expression or relatively complex stimulation strategies[4–7] (but see [9]).

Correspondence: Rafael Yuste, Department of Biological Sciences, Columbia University, 906 NWC Building, 550 West 120 Street, Box 4822, New York, NY 10027. (212) 854-2354 phone, (212) 854-4619 fax. rafaelyuste@columbia.edu.

*Both authors contributed equally

Present Addresses A.M.P.: Wolfson Institute for Biomedical Research, University College London, Gower Street, London WC1E 6BT, UK

Note: Supplementary information is available in the online version of the paper.

Author contributions

A.M.P., D.S.P. and R.Y. designed and built the microscope software and hardware. A.M.P., D.S.P., and J.J.H. performed experiments, data analysis and quantification. R.P. and K. D. provided viral constructs, technical assistance, advice and opsin characterization. A.M.P., D.S.P., J.J.H. and R.Y contributed to the writing of the manuscript.

Competing financial interests

The authors declare no competing financial interests.

To practically combine two-photon microscopy with optogenetics, we sought to make it possible to activate single cells expressing moderate levels of opsins with standard (galvanometer-based) scanning microscopes. We used $C1V1_T$, a new red-shifted chimeric opsin formed by combining *ChR1* and *VChR1*[1], which has significant two-photon absorption above 1,000 nm and slower channel kinetics[10]. We infected the somatosensory cortex of adult mice with AAVs containing *$C1V1_T$* and *EYFP*, under the control of the CaMKII promoter, and after four weeks made neocortical slices and performed two-photon imaging on them (Fig. 1a, see Online Methods). We found large cortical territories with EYFP-labeled neurons, which were assumed to also express $C1V1_T$ (Fig. 1b). The area with EYFP-expressing cells extended over 1,200 μm with strongest expression over the central 750 μm zone, particularly in cortical layers 2, 3 and 5. Using two-photon imaging, we could identify individual neuronal somata, dendritic and axonal processes across all cortical layers (Fig. 1c–d). We patched fluorescently labeled cells and first activated these neurons with blue light (mercury arc lamp, bandpass 470–490 nm, 20X 0.5NA objective, 0.3 mW/mm^2 on sample) while measuring currents by voltage-clamp. Photostimulated currents exhibited a large range of steady-state one-photon currents even near the highest expression area (754 ± 53 pA, range 40–1870 pA, n = 58, Fig. 1e). We then performed two-photon stimulation (1064 nm) of targeted cells by raster-scanning a small square region of interest (ROI) on the cellular somata. Increasing the light power on the sample from 1–41 mW produced stronger currents, which saturated at hundreds of picoamperes (Fig. 1f). For individual neurons, the ratio of photocurrents produced by wide field one-photon excitation to those produced by two-photon somatic restricted ROI-scanning (30 mW) was nearly constant (6.9 ± 2.8, n = 12; *mean* ± *SD*; R = 0.76). Because of this, one-photon photocurrents can predict two-photon responses.

We optimized the two-photon scanning parameters to produce the highest peak photocurrents (Fig. 1g; see Methods), and chose 2 milliseconds/line scanning of a 32×32 square pixel ROI as the optimal scanning profile (which results in a 73.4 millisecond photostimulation). This protocol reliably generated action potentials (APs) in current-clamp recordings (Fig. 1h). The spatial resolution of the two-photon stimulation using this scanning pattern enabled single-cell precision in firing of individual cells (FWHM = 6.5 μm lateral resolution, 20 μm axial resolution; Supplementary Fig. 1). Generally, only one AP was generated per raster-scan (1.18 ± 0.56; mean ±SD n = 795 photostimulations), although neurons expressing high levels of opsin (as inferred from their high one-photon photocurrents; >1nA) sometimes produced two or three APs under two-photon stimulation. Latencies from the start of the scan to the peak of the first AP were reproducible across cells (58 ± 12 milliseconds; mean ±SD n = 16 cells; Fig. 1h), and were shorter with both increased expression and increased light-power on the sample (R = 0.2 and 0.4; data not shown). The AP jitter, defined as the standard deviation of the latency, was 11 ± 7.7 milliseconds (mean ±SD; n = 15 cells). AP latency increased with subsequent stimulations under excitation frequencies of >0.1 Hz (R^2=0.8; Fig. 1i). Prolonged photostimulation produced APs at frequencies exceeding those of four times rheobase (Fig. 1j).

We then used two-photon illumination of $C1V1_T$ to stimulate single dendrites and spines. We selected cells exhibiting high EYFP expression and raster-scanned individual dendritic

processes, using the same patterns used to successfully generate photocurrents in somata (23 pA ± 11 pA, mean ±SD range 7–49 pA, *n* = 21 dendrites, 8 neurons; Fig. 2a). Dendrites located further from the soma yielded lower currents (R^2=0.2; Supplementary Fig. 2). We also targeted spines and dendrites with point excitation, which elicited smaller currents (Fig. 2b, Supplementary Table 1). We did not elicit photocurrents when we moved the laser a few microns away from the targeted spines or dendrites (Supplementary Fig. 3). Mean peak currents for point stimulation were similar for spines (7.1 ± 1.58 pA; mean ±SD *n* = 8) and dendrites (6.0 ± 1.14 pA; mean ±SD *n* = 5; Mann-Whitney, *p* = 0.33). Mean 10–90% rise time was also similar for spines (15.5 ± 4.16 milliseconds; mean ±SD *n* = 8) and dendrites (15.6 ± 5.73; mean ±SD *n* = 5; Mann-Whitney, *p* > 0.99). Latencies for point photostimulation of spines and dendrites were always less than 3 milliseconds (Supplementary Table 1) and decay kinetics were also similar, over 60 milliseconds (data not shown). Spines and dendrites of very weakly or non-expressing cells (*n* = 4), showed no response under identical photostimulation conditions (*n* = 3 spines and 3 dendrites; data not shown).

A useful application of two-photon photostimulation is optical mapping of synaptic circuits[3], so we explored whether this was possible with $C1V1_T$. We patched pyramidal neurons (*n* = 36), and monitored time-locked excitatory postsynaptic currents (EPSCs) while raster-scanning cell bodies of neighboring EYFP-fluorescent cells, to identify presynaptically connected neurons (Supplementary Fig. 4). Indeed, we found many instances where photostimulating a neuron generated time-locked EPSCs in the patched cell (Fig. 2c). Increasing laser power often revealed time-locked EPSCs from neurons which originally did not generate them, presumably by inducing the presynaptic neuron to spike (Supplementary Fig. 5). We tested 169 possible presynaptic neurons, of which 8 were identified as connected to the post-synaptic cell, based on the kinetics of the time-locked EPSCs generated. In these cases, the amplitude and rise-time kinetics of optically-evoked EPSCs matched that of monosynaptic EPSCs observed between pairs of connected pyramidal neurons, targeted randomly (Supplementary Fig. 6a; EPSCs amplitudes: 17.5 ± 12.8 pA, mean ±SD *n* = 16 pairs, for paired-recordings vs. 15.6 ± 12.7 pA, mean ±SD *n* = 8, for optically stimulated; *p* = 0.72, *t*-test; EPSC risetime 2.17 ± 0.69 milliseconds, mean ±SD *n* = 16, for paired-recordings vs. 2.3 ± 1.1 milliseconds, mean ±SD *n* = 8, for optical stimulated; *p* = 0.54, Mann-Whitney). Currents generated by direct stimulation of the postsynaptic cell's dendritic arbor were easy to distinguish from EPSCs because the rise times and latencies did not overlap (Supplementary Fig. 6). These differences—and the high spatial resolution of the system (Supplementary Fig. 1)—implied accurate detection of presynaptic neurons. We confirmed this by patching putative presynaptic neurons (Fig. 2d), as well as putatively unconnected ones. Every electrically tested pair matched the optical prediction (*n* = 5, 2 connected, 3 unconnected). In one connected pair, hyperpolarizing the presynaptic cell prevented optical activation and the appearance of time-locked EPSCs, confirming that the patched connected neuron was the unique source of the observed current (Supplementary Fig. 7). Finally, we photostimulated two putative presynaptic neurons with brief (12 ms) interstimulation intervals. This generated trains of postsynaptic EPSCs (inter EPSC intervals range 81 – 168 ms), with a paired-pulse ratio (PPR) of 0.68 ± 0.03 (mean ±SD *n* = 2 neurons, Supplementary Fig. 8). This synaptic depression is often found in

neocortical excitatory connections[3], so it may be possible to optically map short-term synaptic plasticity using this methodology.

Lastly, we explored the use of C1V1$_T$ for two-photon spatial light modulator (SLM)-based microscopy, a holographic method that enables optical targeting groups of neurons or spines located in arbitrary 3D positions[11, 12]. We first projected two laser beams of equal power onto two C1V1$_T$-expressing cells, and confirmed that action potentials were generated simultaneously in both cells with paired recordings (Fig. 3a; *n* = 6 pairs). Increasing the number of optically targeted neurons to 15 could still reliably trigger action potentials in the monitored cells (n = 3), and we confirmed that similar light powers were delivered to each of the 15 positions (Fig. 3a, right; Supplementary Fig. 9; Online Methods). We then used SLM targeting to perform 3D photostimulation of neurons. We first patched a C1V1$_T$-expressing neuron, moved the objective to a different focal plane, and photostimulated the cell with an SLM pattern (single or multiple spots) calculated to focus at the cell's plane. Using this approach, APs were reliably generated in neurons positioned at axial planes different than the objective (*n* = 7 neurons; Fig. 3b), confirming that focusing the laser beam with the SLM did not degrade its resolution. We then performed dual whole-cell recordings from neurons located at two different depths (Δz ~ 20 μm) and split the laser beam into two independent beamlets of equal power. When the beamlets were targeted to a single focal plane, coinciding with one of the two neurons, only that neuron generated an AP (Fig. 3c). But when we targeted the beamlets to both planes we were able to elicit action potentials in both neurons simultaneously (Fig. 3d). This shows that, by altering the SLM pattern and without refocusing the objective, we can independently photostimulate two cells located in different planes without cross stimulation (n = 2 pairs).

Using C1V1$_T$ and standard two-photon laser scanning we demonstrate an efficient combination of optogenetics and two-photon microscopy, enabling precise activation of individual neurons and dendritic spines. The method also allows optogenetic-based mapping of presynaptic neurons and may permit studies of synaptic weights and dynamics. Finally, by generating multiple laser beams with SLMs, several neurons can be selectively or simultaneously activated in 3D, an approach that could enable the optical dissection of the function of microcircuits with single cell precision.

Methods and any associated references are available in the online version of the paper.

Online Methods

Viral infection, slice preparation, and electrophysiology

Animal handling and experimentation was done according to the National Institutes of Health and local Institutional Animal Care and Use Committee guidelines. Animals of both sexes were used and were housed and maintained in a temperature-controlled environment, on a 12-hour light- dark cycle, with ad libitum food and water in a Columbia University Animal Facility. We injected C57BL/6 mice aged P21-P24 with 750–850 nL of AAV-CamKII-C1V1T(E162T)-p2A-EYFP at a rate of 130 nL/min at a depth of 400 μm from the pial surface of the somatosensory cortex using a UMP3 microsyringe pump (World Precision Instruments). After waiting at least four weeks, acute coronal slices 350 μm thick

were prepared from P57-210 mice using a Leica VT1200S vibratome following cardiac perfusion with ice-cold sucrose solution containing the following (in mM): 27 $NaHCO_3$, 1.5 NaH_2O_4, 222 sucrose, 2.5 KCl, 3 $MgSO_4$, and 1 $CaCl_2$. Slices were incubated at 36°C for 30 min in ACSF containing (in mM): 126 NaCl, 26 $NaHCO_3$, 1.1 NaH_2O_4, 10 glucose, 3 KCl, 3 $MgSO_4$, and 1 $CaCl_2$. During recordings, ACSF was similar except for (in mM): 2 $MgSO_4$ and 2 $CaCl_2$. Sucrose and ACSF solutions were saturated with 95% O_2 and 5% CO_2. Whole-cell recordings were made through 5–6 MOhm glass pipettes using Axon Multiclamp 700B amplifiers (Molecular Devices), digitized at 10 KHz with National Instruments 6259 multichannel cards, and recorded using custom software written using LabView (National Instruments). Intracellular solution, pH 7.2, contained (in mM): 135 K-methylsulfate, 8 NaCl, 10 HEPES, 2 Mg-ATP, 0.3 Na-GTP, 7 phosphocreatine, 0.02 Alexa Fluor 594, and 10.7 biocytin.

Imaging and photostimulation

Experiments were performed with a custom-made two-photon dual-laser dual-scanning microscope based on a modified Olympus BX50WI microscope with a 40× 0.8 NA or 20× 0.5 NA water-immersion objectives (Olympus). Initial photostimulation characterization and mapping experiments were performed using a Ti:sapphire laser as the light source (Coherent Chameleon Ultra II, 140 fs pulses, 80 MHz repetition rate). These experiments using the Ti-Sapphire were performed at 1040 nm. Scanning was performed using one of the set of galvanometer mirrors controlled using Fluoview software (Olympus). This scanning system had a low fill fraction (the amount of time spent scanning the marked ROI versus the total scan time) and though successful in triggering action potentials, it was relatively inefficient, with low peak photocurrents and large jitter and latency.

All other experiments were performed with a second set of scanners on our two-photon laser-scanning and SLM microscope[11]. The laser for this microscope was fixed at 1064 nm and produced 300 fs mode-locked pulses (Fianium 1060 FS-5; 1064 nm, 5W, 300 fs, 80 MHz). Galvanometers mirrors (Cambridge Technology) and a reflective HD SLM (Holoeye 1080 HEO) were installed with the mirrors controlled by ScanImage (Janelia Farm) and the phase mask sent to the SLM via software from Holoeye. Care was taken to ensure raster scans had a high fill fraction to minimize stimulation outside the selected ROI. Optimal raster scans (2 ms/line, Fig. 2c) were performed bidirectionally over neuronal cell bodies (32 by 32 pixels, 51.2 μs dwell time per pixel).

Two-photon activation of C1V1$_T$- expressing neurons

To optimize AP generation, we explored the power dependency of the two-photon photocurrents. We obtained significant currents with as little as 1 mW of 1064nm light on sample (20X 0.5 NA objective) whereas currents saturated above ~30mW at a level dependent on the amount of opsin expression. We also optimized the temporal pattern of the photoactivation. For short duration illuminations, the off-time of C1V1$_T$ is ~60 ms (ref. 10), but this may depend on illumination time and intensity. In our experiments, using more extended illuminations (150 ms), we measured an effective off-time of ~ 80 ms, and chose this as our upper bound for effective scan times. Since the diameter of a typical neuronal soma is ~15–20 μm and the effective PSF produced with the 0.5 NA objective at non-

saturating powers is ~1 μm, we chose to scan the cell ROI with 32 lines, ensuring the complete overlapped coverage of the entire cell. At typical excitation powers (30 mW), values of 0.5 ms/line (17 ms per scan) or shorter were too fast to reach the maximum possible current, perhaps due to insufficient integrated photon fluxes for complete activation of all opsins in the selected volume. Meanwhile, values 4 ms/line or longer (>130 ms per scan) were too slow, since, as expected, opsins stimulated in the initial part of the scan were closed before the end of the scan (Fig. 1g). Intermediate scan rates of 1–2 ms/line produced higher, nearly identical, photocurrents. Given that the ratio of one-photon to two-photon photocurrents is 7:1, and the rheobase of a typical pyramidal neuron is around 100 pA[13], the expected average one-photon photostimulation current required for successful two photon activation would be approximately 700 pA. Using the photocurrent histogram (Fig. 1e), we estimate that our two-photon stimulation protocol should fire almost 50% of the excitatory neurons at the injection site. This is likely a lower estimate, as many cells with one-photon currents less than 700 pA were two-photon addressable (Supplementary Fig. 10a). In layers 2, 3 and 5, where we found high C1V1T expression, this would imply that, for a single injection, ~10,000 neurons are capable firing following two-photon photoactivation (48% of all neurons in a sphere 750 μm in diameter, assuming a density of 92,000 neurons per mm[14]). The mean time of expression of animals in our experiments was 8 ± 2 weeks, but we found no strong correlations of photocurrents with time over that window (Supplementary Fig. 10b). Nevertheless, it is possible that with significantly longer expression times there could be an even a larger pool of two-photon addressable cells. However, we did not find this in the oldest acute slices (>30 weeks post injection), which showed a reduced number of EYFP expressing cells, and generally reduced viability, perhaps simply due to the age of the animals. Regardless, with judicious choices of photostimulation parameters, single action potentials were reliably generated in a large fraction of $C1V1_T$-expressing neurons with precise timing using two-photon excitation and simple raster-scanning illumination patterns.

We noticed that trains of photostimulation altered the latencies of the generated APs. The difference between the latency of the first and last AP during a sequence of stimulations (normalized to the latency of the last action potential) was 25 ± 1% during an inter stimulus interval (ISI) of 1 second but dropped to 4 ± 8% with an ISI of 22 seconds. Most neurons appeared to recover their original latencies given sufficient time, indicating that there is a small, subtle photo-induced process that alters the excitability of the cell that recovers on the time scale of seconds, although a very small subset of apparently otherwise healthy cells appear to become resistant to further photostimulation, even with increased power.

Detection of connections after photostimulation

To accurately predict putative presynaptic neurons we needed definitive criteria to distinguish monosynaptic EPSCs from currents generated by directly stimulating the dendrites of the postsynaptic neuron. The rise times for direct stimulations was 35.8 ± 19.4 milliseconds (n = 21), more than ten times the rise times for EPSCs and statistically distinct from them ($p<0.0001$, unpaired t-test). However, the quickest way to distinguish these responses was by the latency of the response from photostimulation onset: all direct photostimulations started within 3 milliseconds of laser onset, while the optically evoked EPSC latency was 54.1 ± 18.6 milliseconds (n = 8, range 29–84 milliseconds). The *smallest*

optically evoked EPSC latency was ten times larger than the *largest* direct stimulation of the postsynaptic cell's arbor, so the statistical difference between these distributions is very strong ($p<0.0001$, unpaired two-tailed t-test). Although we occasionally observed combined events in which a connected presynaptic neuron and a portion of the postsynaptic neuron's arbor were photostimulated simultaneously (Supplementary Fig. 5d), the EPSC trace was easy to identify due to the time-locked nature with which it occurs relative to laser onset and the very different kinetics from direct stimulation.

The average probability of connection found, 5%, is lower than in younger animals[13], although our data is the first we are aware of to probe excitatory connectivity at a large scale in older animals. This low connectivity also indicates that two-photon photostimulation did not cause widespread axonal activation.

SLM Microscopy

In this study, we applied spatial light modulators (SLMs) to generate arbitrary spatiotemporal patterns of light[6, 11, 12, 15–17]. In our setup, the laser beam was expanded to fill the reflective SLM surface, which displayed phase masks that modulated the wavefront of the incoming laser beam such that multiple beamlets were generated in the far-field (e.g. on the sample). Each individual beamlet targeted different neurons within the nominal focal plane of the microscope. These targeted multi-beam patterns were coupled into the microscope through galvanometer mirrors that enabled raster-scanning of the individual laser beam spots across multiple ROIs. Two dimensional phase masks for the SLM were generated by either software provided by Holoeye software or custom code running in Matlab[3], while the three-dimensional patterns were generated exclusively with custom code in Matlab using either a simple prism-lens approach[18] or a paralleled multi-plane optimization algorithm[19].

For individual neurons, the lateral resolution, defined by the full-width at half maximum (FWHM) of the spiking probability, was 6.9 μm and the axial resolution was 29 μm (Supplementary Fig. 6), and was identical to that of normal, single beam targeting with the same objective, confirming that beam splitting with the SLM does not significantly degrade the PSF[11]. The high lateral resolution ensures that, as soon as the cell body was partially outside of the raster-scanned ROI, the spiking probability drops sharply, and implies that it is critical to illuminate a significant portion of the somatic membrane to generate action potentials. As expected, the induced subthreshold photocurrents decayed more slowly (Supplementary Fig. 6A, gray dashed curve). The lower axial resolution was expected, and corresponds to the axial extent of the neuron's cell body convolved with the two-photon PSF generated by the 20X 0.5NA objective. Thus, the SLM microscope was reliable and accurate in generating action potentials in two neurons simultaneously.

To ensure that the optically induced spiking of the single patched neuron would be considered representative of all of the other neurons, we verified that the illumination intensity of the beamlets was identical with subsequent measurements: immediately following the multiplexed optical activation experiments, the sample was changed to a uniformly fluorescent, liquid filled microcapillary (50 μM Rhodamine 6) and illuminated with the same multiplexed, beamlet producing phase masks on the SLM. We measured the

two-photon produced fluorescence generated by each individual beamlet, and observed that there were no significant variations in the intensity of the multiple beamlets (Fig. 3a, right). Based on these measurements, we expect that every one of the additional neurons illuminated by the SLM patterns would fire action potentials, as did the recorded cell. We similarly monitored for "stray" excitation areas, or reductions in the lateral confinement or focusing of the individual multispot targets, and detected no significant effects (Supplementary Fig. 9c–e). Considering our power budget and overall efficiency of our SLM-microscope system - we can deliver almost 1 W on the sample across multiple targets – we anticipate targeting capability for up to 40 pyramidal cells simultaneously within a 500 μm FOV.

Because SLMs are essentially universal optics, they can also act as a focusing lens and the focal position of the laser beam in the sample can be moved independently, in software and without any mechanical devices, relative to the objective's focal plane[11]. The volume that can be addressed by the SLM in our microscope for a given sample and galvanometer mirror position is determined by the SLM pixel pitch and overall effective magnification and was a cylinder 520 μm in diameter and 400 μm tall (20× 0.5NA objective). While there were variations in the PSF through this focused volume, due to changes in the effective NA of the objective because of the additional lens function, and chromatic effects from the diffractive optic (SLM), the effective cell-targeting resolution did not change significantly. Although one would expect more significant degradations with a higher NA, for the purposes of activating somata with two-photon photostimulation, lower NA objectives are actually beneficial[4]. An additional complication of using the SLM as a focusing device is that the nominal magnification factor of the microscope changes as the focal plane is adjusted because the beam is no longer strictly collimated between the tube lens and the objective focal plane. Fortunately, this change is linear and could be easily calibrated (14% increase per focal plane displacement of 100 μm; Supplementary Fig. 9a). Similar effects were recently seen in a novel microscope utilizing an electrotunable lens for fast axial focusing[20]. This change in magnification would begin to affect the lateral resolution of our raster-scanned stimulation protocol if cells were simultaneously targeted and scanned across vastly different axial planes. For these particular instances a more complex stimulation strategy may be required.

In our "out of focal plane" photoactivation experiments there was no apparent change in the axial resolution of action potential generation in the subset of addressable SLM volume that was examined, which was ± 120 μm around the nominal focal plane of the objective (FWHM of action potential probability versus axial distance = 28 ± 5 μm, n = 9 focal planes; steps of 15 μm, in addition to zero lens phase corresponding to objective focal plane). An identical result was seen in an experiment monitoring the peak photocurrents generated by optical stimulation of a cell at different focal planes (Supplementary Fig. 9b).

Supplementary Material

Refer to Web version on PubMed Central for supplementary material.

Acknowledgements

We thank M. Agetsuma and Y. Shin for assistance with viral injections and surgeries and other members of the laboratory for help and comments. R.Y, A.M.P., J.J.H. and D.S.P. are supported by the Howard Hughes Medical Institute, the Kavli Institute for Brain Science, the National Eye Institute, the Keck Foundation, the Deutsche Forschungsgemeinschaft (grant 1728/1-1 to J. J. H.) and the Department of Defense Multidisciplinary University Research Initiative Program. R.P. is supported by National Institute of Mental Health. K.D. is supported by the Howard Hughes Medical Institute, the National Institutes of Health, the California Institute for Regenerative Medicine, the Gatsby Foundation, and the Defense Advanced Research Projects Agency Reorganization and Plasticity to Accelerate Injury Recovery Program.

References

1. Yizhar O, Fenno LE, Davidson TJ, Mogri M, Deisseroth K. Neuron. 2011; 71:9–34. [PubMed: 21745635]
2. Katzel D, Zemelman BV, Buetfering C, Wolfel M, Miesenbock G. Nat Neurosci. 2011; 14:100–107. [PubMed: 21076426]
3. Nikolenko V, Poskanzer KE, Yuste R. Nat Methods. 2007; 4:943–950. [PubMed: 17965719]
4. Rickgauer JP, Tank DW. Proceedings of the National Academy of Sciences of the United States of America. 2009; 106:15025–15030. [PubMed: 19706471]
5. Andrasfalvy BK, Zemelman BV, Tang J, Vaziri A. Proceedings of the National Academy of Sciences of the United States of America. 2010; 107:11981–11986. [PubMed: 20543137]
6. Papagiakoumou E, et al. Nat Methods. 2010; 7:848–854. [PubMed: 20852649]
7. Oron D, Papagiakoumou E, Anselmi F, Emiliani V. Prog Brain Res. 2012; 196:119–143. [PubMed: 22341324]
8. Feldbauer K, et al. Proceedings of the National Academy of Sciences of the United States of America. 2009; 106:12317–12322. [PubMed: 19590013]
9. Zhu P, et al. Front Neural Circuits. 2009; 3:21. [PubMed: 20126518]
10. Mattis J, et al. Nat Methods. 2011; 9:159–172. [PubMed: 22179551]
11. Nikolenko V, et al. Front Neural Circuits. 2008; 2:1–14. [PubMed: 18946541]
12. Lutz C, et al. Nat Methods. 2008; 5:821–827. [PubMed: 19160517]
13. Lefort S, Tomm C, Floyd Sarria J-C, Petersen CCH. Neuron. 2009; 61:301–316. [PubMed: 19186171]
14. Schüz A, Palm G. Journal of Comparative Neurology. 1989; 286:442–455. [PubMed: 2778101]
15. Nikolenko V, Peterka DS, Yuste R. J Neural Eng. 2010; 7:045001. [PubMed: 20644244]
16. Yang S, et al. J Neural Eng. 2011; 8:046002. [PubMed: 21623008]
17. Maurer C, Khan S, Fassl S, Bernet S, Ritsch-Marte M. Opt Express. 2010; 18:3023–3034. [PubMed: 20174133]
18. Daria VR, Stricker C, Bowman R, Redman S, Bachor H-A. Applied Physics Letters. 2009; 95:093701.
19. Piestun R, Shamir J. Significance. 2002; 90
20. Grewe BF, Voigt FF, van 't Hoff M, Helmchen F. Biomedical optics express. 2011; 2:2035–2046. [PubMed: 21750778]

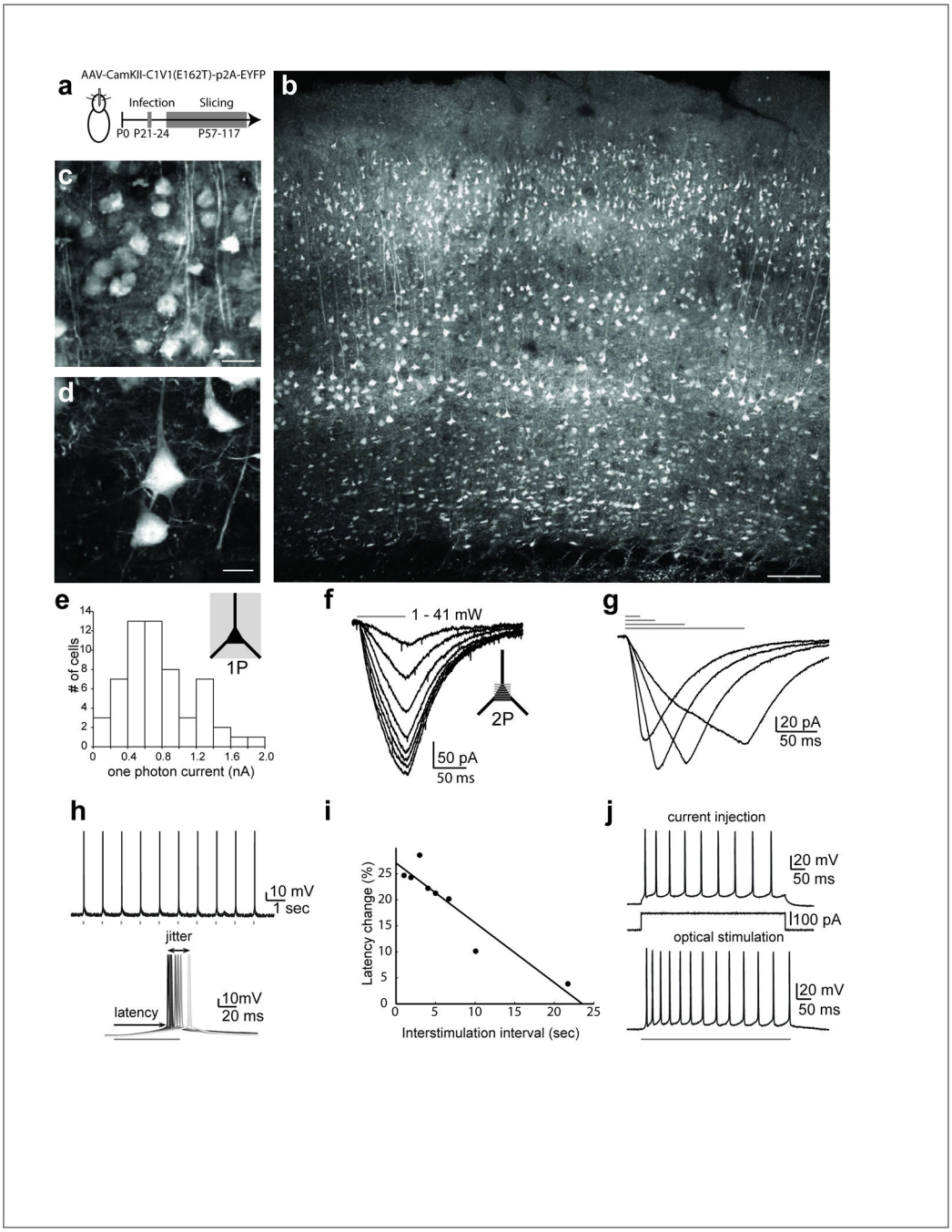

Figure 1. Two-photon activation of individual neurons with C1V1$_T$ in mouse brain slices

(**a**) Experimental strategy. AAVs encoding for the opsin C1V1$_T$ and EYFP- genes are injected into the somatosensory cortex of a mouse. Several weeks later, brain slices are made from the infected region. (**b**) Two-photon fluorescence image of a living cortical brain slice expressing EYFP (940 nm excitation, 15 mW on sample, 25× 1.05 NA objective, scale 100 μm). (**c, d**) Higher magnification images from (**b**) showing C1V1$_T$-expressing cells in upper and lower layers (Scales c: 20 and d: 10 μm). (**e**) Distribution of steady-state currents, elicited by one-photon widefield stimulation, measured with voltage clamp recordings from

C1V1$_T$-expressing cells (Hg arc lamp, bandpass 470–490 nm, 20× 0.5NA objective, 300 μW/mm^2, 150 msec illumination time). Gray box illustrates stimulated area. (**f**) Two-photon photocurrents measured with voltage clamp in a C1V1$_T$-expressing neuron under different illumination light-powers. Raster scan pattern (inset, gray lines) across a neuronal cell body had 32 lines, 2ms/line, and bidirectional scanning (1064 nm, 1–40 mW on sample, 20× 0.5NA objective). (**g**) Two-photon photocurrents induced in C1V1$_T$-expressing neurons under different scan duration times (gray lines correspond to 0.5, 1, 2 and 4 ms/line; same experimental parameters as **f**). (**h**): Top: current clamp recordings from C1V1$_T$-expressing neurons during two-photon illumination (tick marks; same experimental parameters as **f**). Note reliable generation of action potentials (APs). Bottom: Overlay of APs generated by two-photon illumination (grey bar).(**i**). Quantification of AP latency changes from similar experiments as (**h**) with different stimulation intervals. (**j**) Spiking patterns resulting from current injection at four times rheobase (top) and optical stimulation produced by continually raster scanning the cell body for the same time (bottom; otherwise same experimental parameters as **f**).

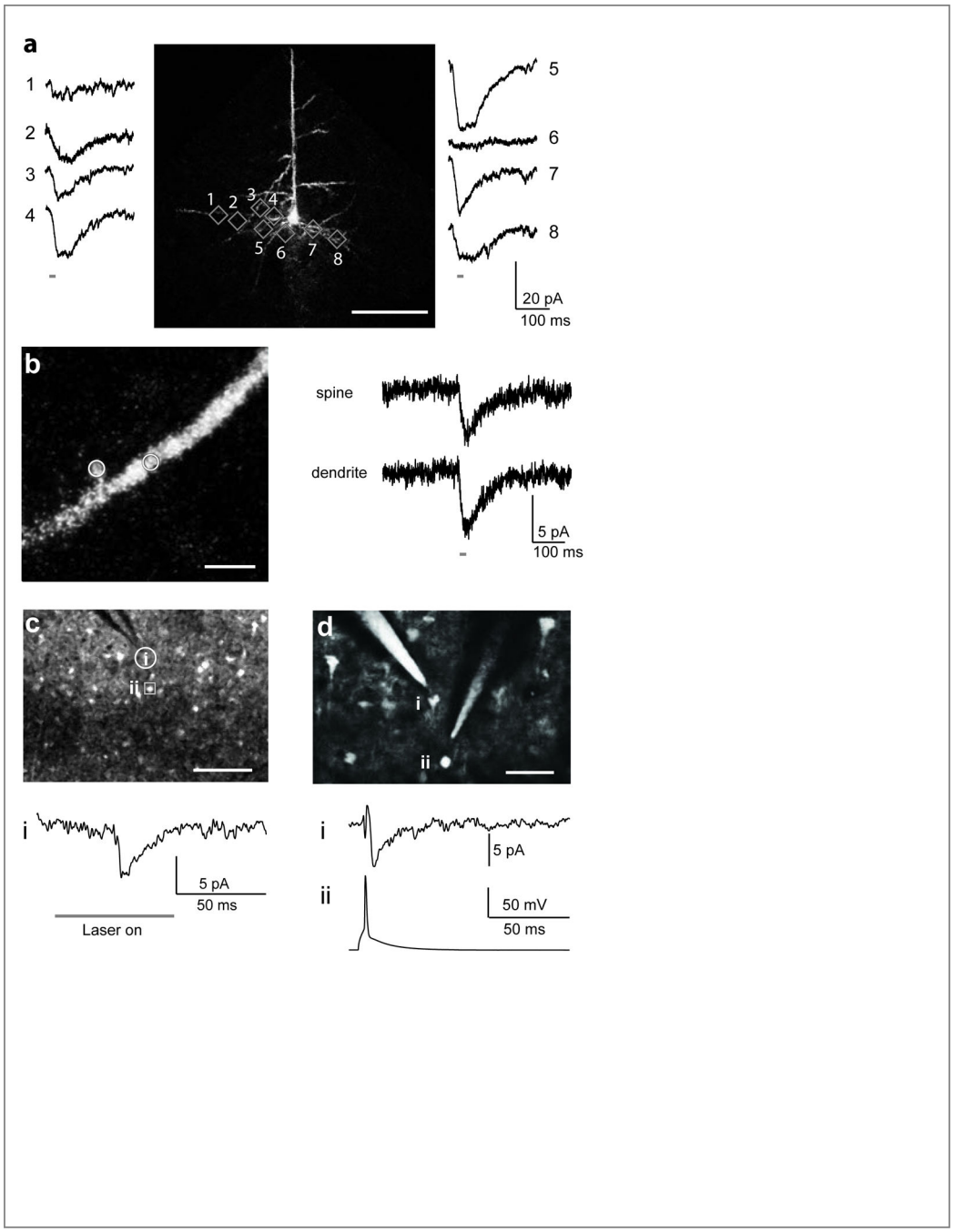

Figure 2. Two-photon stimulation of individual dendrites and spines and optical mapping of connected neurons

(**a**) Photostimulation of cellular processes. Center: two-photon fluorescence image of a C1V1$_T$-expressing neuron (940 nm, 15 mW on sample, 20× 0.5 NA objective). The cell was patched and different regions of its dendritic and axonal arbor were scanned with a two-photon laser (numbered boxes), while somatic currents were simultaneously measured (left and right traces). Photostimulation parameters: 1064 nm, 30 mW on sample, 20× 0.5NA, 32×32 ROI and 2 msec/line. Scale 100 μm. (**b**) Similar experiment as (**a**), but scanning a

spine head and dendritic shaft from a highly expressing neuron (left, scale 3 μm). Imaging parameters as in (**a**). Right: whole-cell measurements of somatic currents during scanning (gray bar; averages of 12). Photostimulation parameters: 1064 nm, 30 mW on sample, 20× 0.5NA and 30 msec point stimulation. (**c**) Mapping presynaptic connections. Top: two-photon fluorescence image of field of neurons expressing $C1V1_T$ (940 nm, 15 mW on sample, 20× 0.5 NA objective). Neuron “i” was patched and surrounding fluorescent neurons were photostimulated, while ESPCs in neuron “i” were monitored. . Scale, 100 μm. Photostimulation parameters: 1064 nm, 30 mW on sample, 20× 0.5NA, 32×32 ROI and 2 msec/line. Bottom: EPSCs in neuron i during photostimulation of neuron ii (average of 12). (**d**) Same experiment as (**c**), after dual whole-cell recording was established from neuron ii. Top: Two-photon fluorescence image from both neurons with identical imaging parameters as (**c**). (Scale, 50 μm). Bottom: Simultaneous voltage-clamp recording from neuron i and current-clamp recordings form neuron ii. .

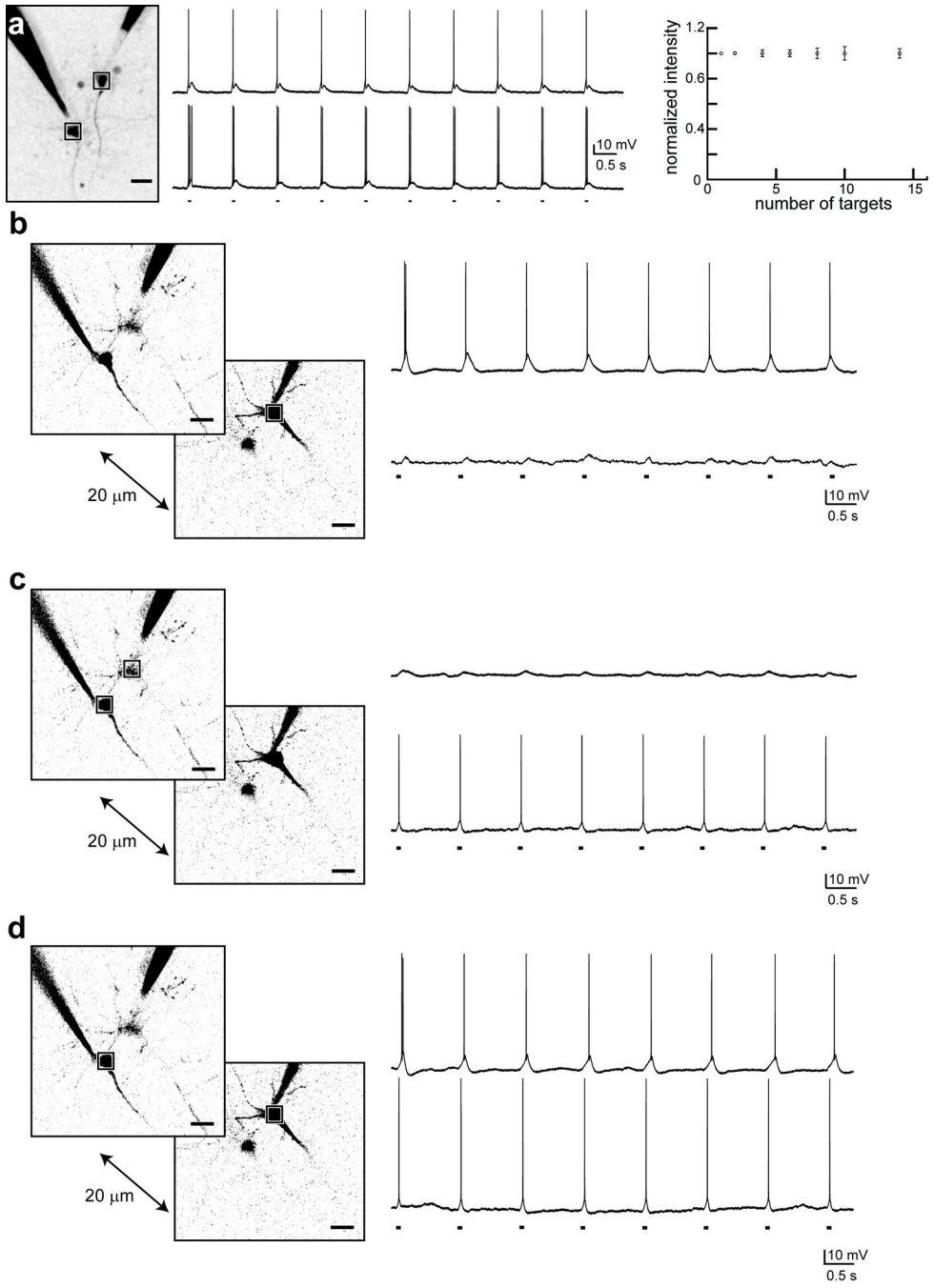

Figure 3. Two-photon 3D stimulation of two individual neurons with SLMs

(**a**) Left: Two-photon fluorescent image of two C1V1$_T$-expressing neurons located in the same focal plane, which were patched. Imaging parameters: 940 nm, 15 mW on sample, 20× 0.5 NA objective. Image look-up table is inverted for clarity. An SLM phase mask was calculated to generate one photostimulation laser spot for each cell, and both laser spots were then raster-scanned simultaneously across the cell bodies (Boxes). Photostimulation parameters: 1064 nm, 30 mW per target, ROI 32×32, 2 msec/line. Middle: Whole-cell current clamp recordings from both cells during two-photon SLM photostimulation (black

marks). Right: Light intensity generated by different number of SLM targets in similar experiments (see Supplementary Fig. 9 for details; 3–15 measurements per target; error bars are SD). (**b**) Depth selectivity of SLM photostimulation. Left: Two-photon fluorescent image of two C1V1$_T$-expressing neurons, located 20 μm apart in depth, which were patched. A single-beam SLM stimulation spot was scanned (box). Imaging parameters as in (**a**). Right: whole-cell current clamp recordings from both neurons during photostimulation of one of them (black marks; black box in left) with the SLM spot. Photostimulation parameters: 1064 nm, 30 mW in one target, ROI 32×32, 2 msec/line. (**c**) Same experiment as in (**b**) but now using a two-dimensional two-beam SLM pattern. Left: Two-photon fluorescent image of two neurons. Imaging as in (**a**). A new SLM pattern is scanned in the superficial focal plane in the position corresponding to the two cells (boxes). Right: simultaneous dual whole cell recordings during photostimulation (black marks). Photostimulation parameters: 1064 nm, 30 mW per target, ROI 32×32, 2 msec/line. This generates (**d**) Same experiment as in (**c**) but with a three-dimensional SLM pattern, which directed two laser beam spots onto both cells simultaneously. Left: Two-photon fluorescent image of both neurons illustrating the simultaneous, multifocal SLM stimulation (boxes). Same imaging parameters as in (**c**). Right: simultaneous dual whole-cell recordings during photostimulation (black marks). Same photostimulation SLM parameters as in (**c**). .